THE JOURNAL OF PHYSICAL CHEMISTRY LETTERS
A JOURNAL OF THE AMERICAN CHEMICAL SOCIETY

pubs.acs.org/JPCL

Letter

Slow Passivation and Inverted Hysteresis for Hybrid Tin Perovskite Solar Cells Attaining 13.5% via Sequential Deposition

Efat Jokar, He-Shiang Chuang, Chun-Hsiao Kuan, Hui-Ping Wu, Cheng-Hung Hou, Jing-Jong Shyue, and Eric Wei-Guang Diau*

Cite This: *J. Phys. Chem. Lett.* 2021, 12, 10106−10111

Read Online

ACCESS | Metrics & More | Article Recommendations | Supporting Information

ABSTRACT: Herein, we report a sequential deposition procedure to passivate the surface of a hybrid mixed cationic tin perovskite (E1G20) with phenylhydrazinium thiocyanate (PHSCN) dissolved in trifluoroethanol solvent. The photoluminescence lifetime of the PHSCN film was enhanced by a factor of 6, while the charge-extraction rate from perovskite to C_{60} layer was enhanced by a factor of 2.5, in comparison to those of the E1G20 film. A slow surface passivation was observed; the performance of the PHSCN device improved upon increasing the storage period to attain an efficiency of 13.5% for a current−voltage scan in the forward bias direction. An inverted effect of hysteresis was observed in that the efficiency of the forward scan was greater than that of the reverse scan. An ion-migration model as a result of the effect of the phenylhydrazinium surface passivation is proposed to account for the observed phenomena. The device was stable upon shelf storage in a glovebox for 3000 h.

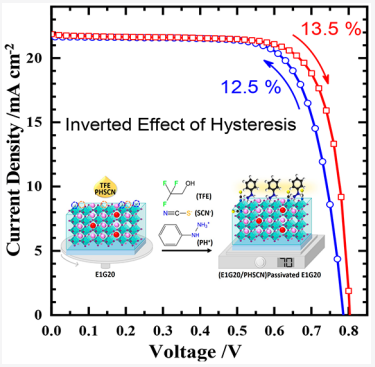

Perovskite solar cells (PSCs) have attracted much attention in recent years as a result of their great performance, comparable to that of Si-based solar cells,[1−3] but traditional PSCs contain toxic lead that restricts their industrial development.[4] For this reason, tin-based PSCs appear to be prospective candidates for the development of lead-free PSCs.[5,6] The preferential device architecture of a Sn-based PSC has a p-i-n inverted configuration as a result of its favorable charge transport against tin oxidation.[7] Since its rapid progress beginning from 2016, the efficiency of power conversion (PCE) of an inverted Sn-based PSC has been greatly enhanced from 6.22% to a new milestone, PCE of 14.81%, with negligible hysteresis.[8,9] Many strategies have been applied to improve the device performance, including formation of two-dimensional (2D)/three-dimensional (3D) structures and with additives as antioxidizers,[10−21] surface passivators,[20] crystallization regulators, etc.[22,23] Among those promising additives, phenylhydrazinium halides (PHX) play an important role to prevent Sn(II)/Sn(IV) oxidation to greatly enhance the performance and stability of Sn-based PSCs.[17,24] In that approach, the phenylhydrazinium (PH) cation was introduced to passivate the trap states of the perovskite film, and the Cl^- anion was incorporated to regulate the nucleation and crystallization. As a result, the PHCl device achieved great efficiency with doping of the Br^- anion.[24] Crystallization regulator NH_4SCN was added to the precursor solution to decrease the density of defects of the perovskite film for an enhanced open-circuit voltage (V_{OC}) attaining 0.94 V.[25] These techniques are, however, all based on a one-step perovskite deposition method, with the key reagent or passivator treated as an additive in the perovskite precursor solution, so that control of the surface passivation becomes difficult.

We previously fabricated Sn perovskite ($FA_{0.8}GA_{0.2}SnI_3$, abbreviated as E1G20) films, with a 3D/2D architecture according to a two-step sequential approach to attain PCE of 10.6% with great stability.[11,26] In that work, the 2D layer was produced on top of the E1G20 film in the second step using solvent hexafluoropropanol (HFP)[27] because the traditional solvent, isopropyl alcohol (IPA), would damage the tin perovskite film.[11] In the present work, the E1G20 film was further treated with a new surface passivator, phenylhydrazinium thiocyanate (PHSCN), dissolved in a new solvent, 2,2,2-trifluoroethanol (TFE), according to a sequential deposition method described in Figure 1. Because PHSCN has a poor solubility in HFP, TFE was found to be a suitable solvent to dissolve PHSCN effectively and to maintain the E1G20 layer intact. The idea of using PHSCN in the second step of deposition is to have a PH cation as a reducing agent for surface passivation as well as to have a SCN^- anion as a pseudohalide to replace part of the I^- anion for surface protection. As a result, a highly performing Sn-PSC was produced according to a typical inverted device configuration, shown as the inset in Figure 1. Furthermore, the device

Received: September 22, 2021
Accepted: October 8, 2021
Published: October 11, 2021

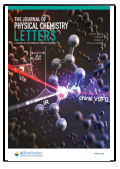

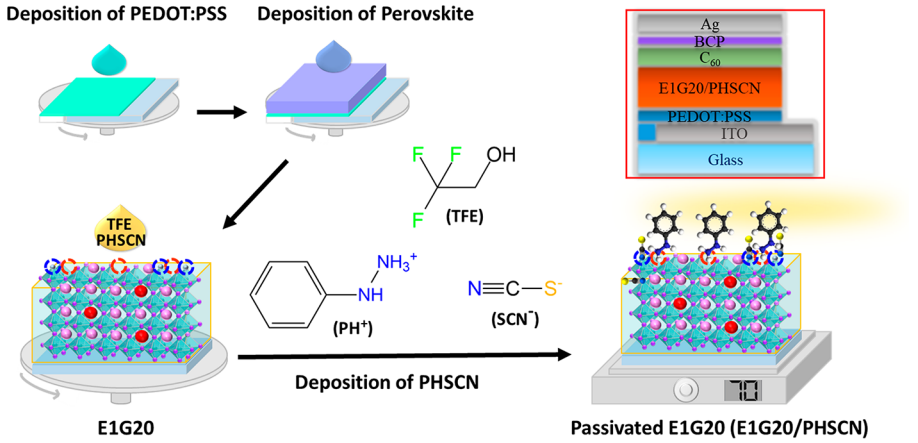

Figure 1. Schematic representation of the E1G20/PHSCN fabrication via sequential deposition. The magenta balls represent FA cations, and the red balls represent the GA cations. The blue and orange dashed circles represent surface defects for SCN^- and PH^+ to occupy, respectively. The red box indicates the inverted planar device structure of the present work.

performance increased slowly upon storage in a N_2-filled glovebox to attain PCE of 13.5%; a fascinating effect of inverted hysteresis was also observed, all described in what follows.

The scanning electron microscopy (SEM) images shown in Figure S1 of the Supporting Information indicate that spin coating of TFE did not alter the morphology of the perovskite film (Figure S1b of the Supporting Information) and that the addition of PHSCN (Figure S1c of the Supporting Information) slightly modified the surface morphology and grain shape because of the change of crystallinity on the perovskite surface. High-resolution X-ray diffraction (XRD) patterns are shown in Figure 2a, in which the diffraction signals of the PHSCN film shifted slightly toward a region of angle smaller than those of the E1G20 film, as shown in the inset of Figure 2a. We expect that a larger SCN^- anion might replace part of the I^- anion on the surface to cause this shift; this anion exchange is limited to the surface or near-surface region. Grazing-incidence wide-angle X-ray (GIWAX) scattering images shown in Figure S2 of the Supporting Information confirm that the shifts in the XRD were limited to only the surface (Figure S2c of the Supporting Information) and not the bulk (Figure S2f of the Supporting Information). No evidence of formation of a low-dimensional perovskite structure was observed, judging from both XRD and GIWAX results. To further validate the component substitution confined to the surface, we undertook time-of-flight secondary ion mass spectral (ToF-SIMS) analysis that provided unambiguously the spatial distribution of each component. The PH^+ and SCN^- distributions tracked by the C_4 and SCN^- signals, respectively, were found to be concentrated on the surface, as shown in the ToF-SIMS depth profile (Figure 2b). The cation or anion replacements were hence restricted to the top-surface region because of limited diffusion dynamics of the PHSCN molecule, coinciding well with the GIWAX results dependent upon the depth shown in Figure S2 of the Supporting Information.

The presence of PHSCN clearly affected the electrical and optical properties of tin perovskite and significantly decreased the defect densities. Because the effect of PHSCN is limited to the surface, the optical properties of E1G20 and a passivated film are identical; the band gap and absorption coefficient show no perceptible change (Figure S3 of the Supporting Information). A substantially improved emission lifetime was observed with a time-correlated single-photon counting (TCSPC) technique, which is direct evidence of successful defect passivation with PHSCN. As shown in Figure 2c, the photoluminescence (PL) decay profiles indicate a clear trend for the average PL lifetimes (Table S1 of the Supporting Information), showing a descending order with PHSCN (10.8 ns) > E1G20 (1.7 ns) > E1G20/C_{60} (1.0 ns) > PHSCN/C_{60} (0.9 ns). The lifetimes of the photoinduced carriers decreased significantly when the electron-extraction layer (C_{60}) was present; both E1G20 and PHSCN films showed a markedly decreased lifetime, but the ability of electron extraction from perovskite to the C_{60} layer was much greater for the PHSCN film than for the E1G20 film (Table S1 of the Supporting Information). We therefore calculated the time coefficient (τ_e) for electron injection according to the equation: $\frac{1}{\tau_e} = \frac{1}{\tau(\mathrm{PSK}/\mathrm{C_{60}})} - \frac{1}{\tau(\mathrm{PSK})}$; the τ_e values of E1G20/C_{60} and PHSCN/C_{60} films were thus determined to be 2.4 and 0.98 ns, respectively. Surface passivation of E1G20 with PHSCN thus shows an enhanced rate of electron extraction from perovskite (E1G20) to the electron transport layer (C_{60}) by a factor of 2.5.

Decreasing the amount of Sn(IV) was observed from X-ray photoelectron spectroscopy (XPS) (Figure S4 of the Supporting Information) as a result of decreasing the defect sites via PHSCN passivation. Lesser p-doping (a lower Fermi level) was also observed in ultraviolet photoelectron spectroscopy (UPS) (Figure S5 of the Supporting Information) for the PHSCN film than for the E1G20 film. Both work function and Fermi-level energies were determined to give the valence band maxima (VBM) shown in Figure 2d. Because the PHSCN treatment does not affect the band gap (Figure S3 of the Supporting Information), both VBM and conduction band minima (CBM) of the PHSCN film shifted upward by 0.1 eV relative to those of the E1G20 film. A satisfactory matching of the potential energy level of the VBM of PHSCN with that of poly(3,4-ethylenedioxythiophene):poly(styrene sulfonate) (PEDOT:PSS) (−5.08 versus −5.1 eV) indicates that charge extraction from perovskite to the hole-transport layer (PEDOT:PSS) should be feasible. Furthermore, the level of CBM of PHSCN being slightly higher than that of E1G20 is consistent with the greater rate of charge extraction observed from PHSCN to C_{60} than from E1G20 to C_{60} (Figure 2c). As a

https://doi.org/10.1021/acs.jpclett.1c03107
J. Phys. Chem. Lett. 2021, 12, 10106−10111

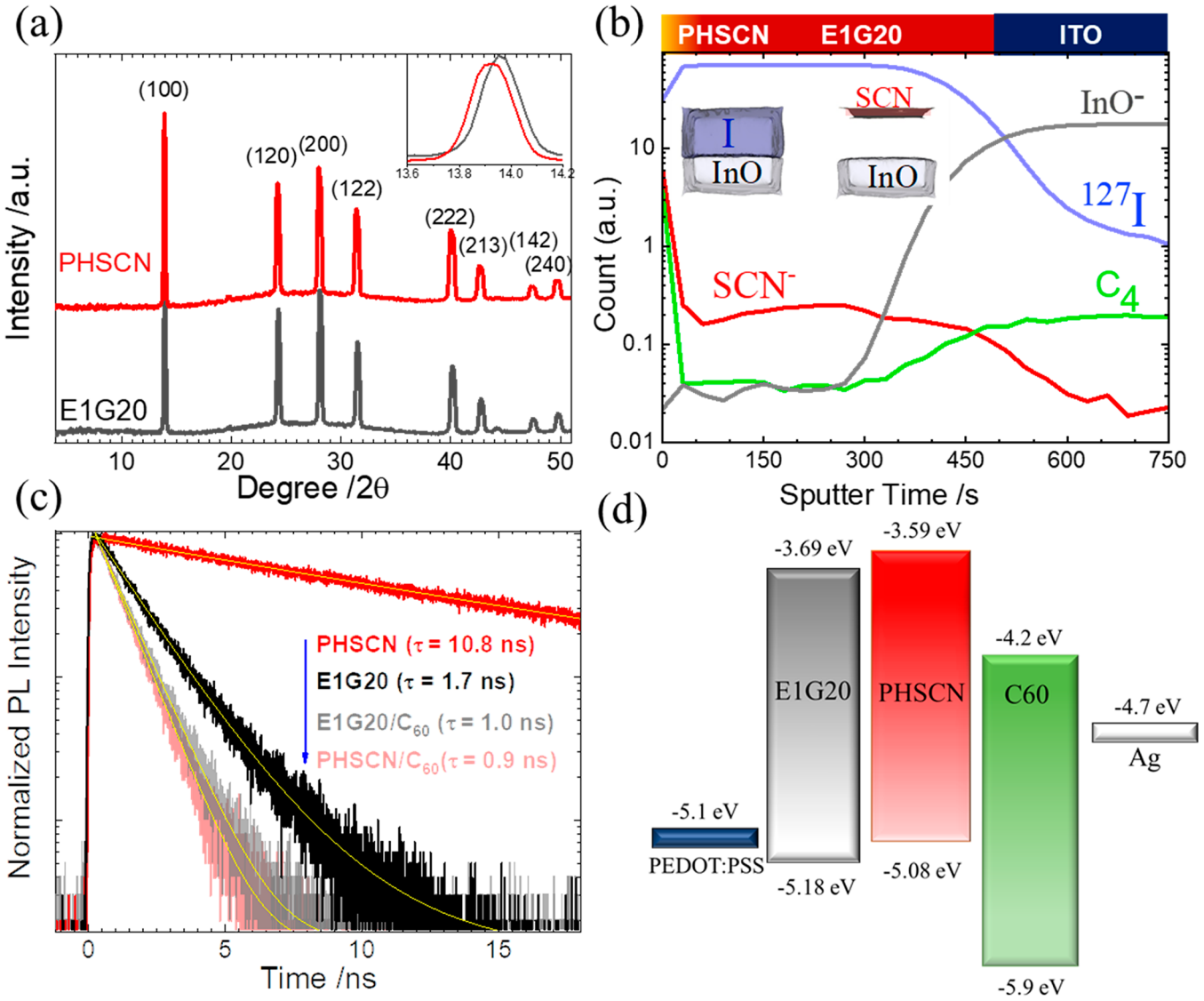

Figure 2. (a) High-resolution XRD patterns of E1G20 and PHSCN films [the inset shows a magnification of two (100) signals for comparison], (b) positive mode of ToF-SIMS spectra of a PHSCN film (3D SIMS images of I^- and SCN^- mapping data are shown in the inset), (c) transient PL decay profiles of perovskite and perovskite/C_{60} films with fitted curves shown as yellow traces with average lifetimes indicated in parentheses in descending order (the transients of the E1G20/C60 and PHSCN/C60 films overlap to some extent, but the two decay profiles can be clearly distinguished with different colors), and (d) potential energy diagrams [energies (eV) with respect to the vacuum level] with energy values of both E1G20 and PHSCN-treated E1G20 films obtained from UPS and absorption spectral data.

result, a greater current was observed in conductive atomic force microscopy (c-AFM) images for the former than for the latter, as shown in Figure S6 of the Supporting Information.

The Sn-PSC devices were fabricated on indium tin oxide (ITO) glass substrates according to an inverted device configuration with architecture ITO/PEDOT:PSS/PHSCN/C60/BCP/Ag shown in the inset of Figure 1. We fabricated 60 E1G20 and PHSCN devices under the same experimental conditions; the corresponding photovoltaic parameters of fresh devices are shown as box plots in Figure S7 of the Supporting Information. In comparison to E1G20 as a reference cell, the PHSCN devices had much improved V_{OC} and fill factor (FF) values with a comparable J_{SC} value [the corresponding external quantum efficiency (EQE) spectra and steady-state current scan at maximum output power are shown in panels a and b of Figure S8 of the Supporting Information, respectively], which gave an overall performance of the PHSCN devices better than that of the E1G20 devices. Significantly enhanced V_{OC} and FF are related to a successful passivation of surface defects by PHSCN; the dark $J-V$ curves (Figure S9 of the Supporting Information) demonstrate smaller current leakage and background charge carrier density for the PHSCN device than for the E1G20 device. When fresh devices were prepared, a superior PCE of 10.9% with V_{OC} of 0.63 V was achieved for the best PHSCN device, while the best E1G20 device gave only PCE of 8.9% and V_{OC} of 0.56 V (Table S2 of the Supporting Information). When the PHSCN device was stored in a nitrogen-filled glovebox, an effect of slow passivation was observed, as shown in Figure 3a. This phenomenon is the same as what we observed previously for the E1 (the form of $FASnI_3$ in the absence of the GA cation) and E1G20 devices with the addition of the ethylenediaminium iodide additive (1%).[15,26] Upon storage, both short-circuit current density (J_{SC}) and FF retained similar values, but V_{OC} increased significantly, leading

https://doi.org/10.1021/acs.jpclett.1c03107
J. Phys. Chem. Lett. 2021, 12, 10106−10111

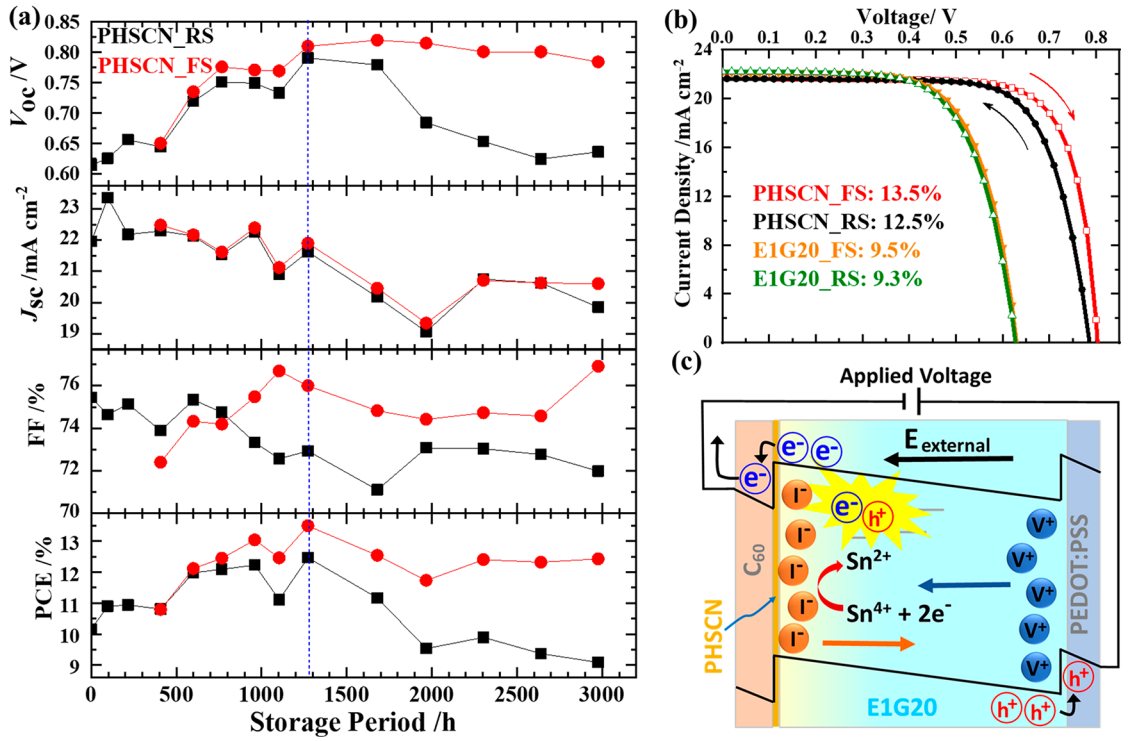

Figure 3. (a) Photovoltaic parameters of a PHSCN device stored in a N_2-filled glovebox as a function of the storage period up to 2978 h; the effect of hysteresis was negligible at the beginning, so that the FS began at 408 h. (b) Current density−voltage characteristics of the best E1G20 and PHSCN devices at the storage period indicated as a blue dotted line in panel a and (c) schematic illustration of operation of a PHSCN device under a bias voltage explaining the inverted effect of hysteresis. The surface passivation of E1G20 by PHSCN led Sn(IV)/Sn(II) oxidation to occur near the n-contact electrode (the C_{60} side), so that iodine anions could accumulate around the n-contact electrode to impede efficient electron transfer and induce charge recombination under a large applied voltage.

to a greatly enhanced PCE with increasing storage period. While measuring the $J-V$ characteristics, we also observed a hysteresis to appear after storage over 600 h, whereas our fresh devices showed negligible hysteresis (Figure S10 of the Supporting Information). Differing from a traditional lead-based PSC, an inverted effect of hysteresis was observed: the forward scan (FS) of the PHSCN device gave better performance than the reverse scan (RS); the $J-V$ curves of both FS and RS of the PHSCN devices are shown in Figure S11 of the Supporting Information. As shown in Figure 3a, the efficiencies obtained from the FS gradually increased and attained maximum performance PCE of 13.5% at 1272 h, which achieves a new milestone for tin-based PSCs (recent reports on device performance are compared in Table S3 of the Supporting Information). Figure 3b shows $J-V$ curves of both FS and RS of both devices that represent the effect of inverted hysteresis for the PHSCN device but no effect for the reference cell E1G20. Han and co-workers also observed such an inverted effect, i.e., higher performance in the FS than in the RS,[28] but proffered no explanation. We discuss this issue in what follows.

The regular effect of hysteresis in Pb-based PSCs was first reported by Snaith and co-workers who suggested that surface defects might act as traps for electrons and holes to be filled under a FS condition, resulting in effective p and n contacts at the interfaces for the RS.[29] Another interpretation by Walker and co-workers was based on a theoretical simulation, for which a slow ion migration might be responsible for the observed hysteresis in C_{60}-based PSCs less than in the TiO_2-based PSCs.[30] In our case, the PHSCN post-treated on the surface of E1G20 had the effect of surface passivation; the SCN^- anion might diffuse slowly into the E1G20 crystal similar to the role played by the $EDAI_2$ additive responsible for the observed effect of slow relaxation of crystal structures. The PH^+ cation served as an agent to reduce Sn(IV) to Sn(II) that requires two electrons for each cycle. We expect that this reduction is the driving force for iodine anions to move toward the surface of E1G20 (n-contact electrode), to fill surface trap states arising from halide vacancies near the n-contact electrode (hole vacancies thus moved near the p-contact electrode). As shown in Figure 3c, application of a large external voltage generated a large external field, so that the trapped iodine anions (perhaps also some SCN^- anions) could move slowly toward the PEDOT:PSS (p contact) direction (the hole vacancies also moved in the reverse direction). Because an accumulation of iodine anions at the n-contact region would effectively impede electron transfer from E1G20 to C_{60}, a large electric field generated with an applied voltage thus released some constraints for the electron transfer to become more efficient. For the FS condition, the applied voltage increased upon the $J-V$ scan; the trapped iodine anions did not move toward the p-contact direction before a threshold value at ∼0.5 V (Figure 3b) was attained, at which the FS began to differ from the RS. For the RS beginning from a large applied voltage, the iodine ions move back toward the n-contact electrode area for the voltage scan to the threshold of ∼0.5 V; this slow ion migration would generate a blocking layer to prevent the electrons from being transported to the n-contact electrode. As a result, charge recombination would occur near the n-contact region, so that less current resulted

https://doi.org/10.1021/acs.jpclett.1c03107
J. Phys. Chem. Lett. 2021, 12, 10106−10111

for the RS than for the FS at an applied voltage larger than ~0.5 V, which reasonably explains the observed inverted hysteresis. In the case of the E1G20 cell, iodine anions can move freely, so that almost no effect of hysteresis was observed (Figure 3b). Our hypothesis about the observed inverted hysteresis is preliminary and requires theoretical studies for verification.

In conclusion, we report herein a new sequential approach to fabricate hybrid tin perovskite (E1G20) solar cells with a post-surface treatment of PHSCN dissolved in trifluoroethanol, which is a key solvent to dissolve PHSCN effectively with adequate solubility and not to damage the sensitive E1G20 film. We found that PHSCN can efficiently passivate the surface of E1G20 and greatly accelerate the rate of electron transport from perovskite to C_{60}. The performance of the PHSCN device gradually improved upon storage, for which the best efficiency, 13.5%, was obtained via a forward $J-V$ scan when the PHSCN device was stored in a N_2-filled glovebox for 1272 h; the device was stable upon shelf storage for 1272 h to reach its maximum performance and retained 92% of the maximum efficiency after storage for 3000 h. We found a significant effect of inverted hysteresis, in that the device performance was poorer for the reverse scan than for the forward scan. An ion-migration model is proposed to interpret this observed inverted hysteresis effect. Further investigation is required to understand such an abnormal phenomenon and to solve this problem for lead-free PSCs to achieve a new milestone.

■ ASSOCIATED CONTENT

Supporting Information

The Supporting Information is available free of charge at https://pubs.acs.org/doi/10.1021/acs.jpclett.1c03107.

Experimental methods, supplementary figures and tables for SEM, GIWAX, XPS, UPS, ultraviolet−visible (UV−vis)/PL, AFM, c-AFM, performance statistics, $J-V$ curves, incident photon-to-current efficiency (IPCE), and summary of reported device performance (PDF)

■ AUTHOR INFORMATION

Corresponding Author

Eric Wei-Guang Diau − *Department of Applied Chemistry and Institute of Molecular Science, National Chiao Tung University, Hsinchu 30010, Taiwan; Center for Emergent Functional Matter Science, National Chiao Tung University, Hsinchu 30010, Taiwan;* orcid.org/0000-0001-6113-5679; Email: diau@mail.nctu.edu.tw

Authors

Efat Jokar − *Department of Applied Chemistry and Institute of Molecular Science, National Chiao Tung University, Hsinchu 30010, Taiwan; Center for Emergent Functional Matter Science, National Chiao Tung University, Hsinchu 30010, Taiwan*

He-Shiang Chuang − *Department of Applied Chemistry and Institute of Molecular Science, National Chiao Tung University, Hsinchu 30010, Taiwan*

Chun-Hsiao Kuan − *Department of Applied Chemistry and Institute of Molecular Science, National Chiao Tung University, Hsinchu 30010, Taiwan*

Hui-Ping Wu − *Department of Applied Chemistry and Institute of Molecular Science, National Chiao Tung University, Hsinchu 30010, Taiwan*

Cheng-Hung Hou − *Research Center for Applied Sciences, Academia Sinica, Taipei 11529, Taiwan;* orcid.org/0000-0002-5150-7106

Jing-Jong Shyue − *Research Center for Applied Sciences, Academia Sinica, Taipei 11529, Taiwan; Department of Materials Science and Engineering, National Taiwan University, Taipei 10617, Taiwan;* orcid.org/0000-0002-8508-659X

Complete contact information is available at: https://pubs.acs.org/10.1021/acs.jpclett.1c03107

Notes

The authors declare no competing financial interest.

■ ACKNOWLEDGMENTS

Taiwan Ministry of Science and Technology (MOST 110-2123-M-A49-001 and MOST 110-2634-F-009-026) and Center for Emergent Functional Matter Science of National Yang Ming Chiao Tung University (NYCU) from the Featured Areas Research Center Program within the framework of the Higher Education Sprout Project by Taiwan Ministry of Education (MOE) supported this research. The National Synchrotron Radiation Research Center (NSRRC), Hsinchu, Taiwan, provided beam time for measurements of high-resolution XRD and GIWAX.

■ REFERENCES

(1) Jeong, J.; Kim, M. M.; Seo, J.; Lu, H.; Ahlawat, P.; Mishra, A.; Yang, Y.; Hope, M. A.; Eickemeyer, F. T.; Kim, M. M.; Yoon, Y. J.; Choi, I. W.; Darwich, B. P.; Choi, S. J.; Jo, Y.; Lee, J. H.; Walker, B.; Zakeeruddin, S. M.; Emsley, L.; Rothlisberger, U.; Hagfeldt, A.; Kim, D. S.; Gratzel, M.; Kim, J. Y. Pseudo-halide anion engineering for α-$FAPbI_3$ perovskite solar cells. *Nature* **2021**, *592*, 381−385.

(2) Kim, G. H.; Kim, D. S. Development of perovskite solar cells with > 25% conversion efficiency. *Joule* **2021**, *5*, 1033−1035.

(3) Murugan, P.; Hu, T.; Hu, X.; Chen, Y. Current development toward commercialization of metal-halide perovskite photovoltaics. *Adv. Opt. Mater.* **2021**, *9*, 2100390.

(4) Maranghi, S.; Parisi, M. L.; Basosi, R.; Sinicropi, A. The critical issue of using lead for sustainable massive production of perovskite solar cells: A review of relevant literature. *Open Res. Eur.* **2021**, *1*, 44.

(5) Tai, Q.; Cao, J.; Wang, T.; Yan, F. Recent advances toward efficient and stable tin-based perovskite solar cells. *EcoMat* **2019**, *1*, No. e12004.

(6) Wu, T.; Liu, X.; Luo, X.; Lin, X.; Cui, D.; Wang, Y.; Segawa, H.; Zhang, Y.; Han, L. Lead-free tin perovskite solar cells. *Joule* **2021**, *5*, 863−886.

(7) Diau, E. W.-G.; Jokar, E.; Rameez, M. Strategies to improve performance and stability for tin-based perovskite solar cells. *ACS Energy Lett.* **2019**, *4*, 1930−1937.

(8) Liao, W.; Zhao, D.; Yu, Y.; Grice, C. R.; Wang, C.; Cimaroli, A. J.; Schulz, P.; Meng, W.; Zhu, K.; Xiong, R. G.; Yan, Y. Lead-free inverted planar formamidinium tin triiodide perovskite solar cells achieving power conversion efficiencies up to 6.22%. *Adv. Mater.* **2016**, *28*, 9333−9340.

(9) Yu, B.-B.; Chen, Z.; Zhu, Y.; Wang, Y.; Han, B.; Chen, G.; Zhang, X.; Du, Z.; He, Z. Heterogeneous 2D/3D Tin-halides provskite solar cells with certified conversion efficiency breaking 14%. *Adv. Mater.* **2021**, *33*, 2102055.

(10) Chen, M.; Dong, Q.; Eickemeyer, F. T.; Liu, Y.; Dai, Z.; Carl, A. D.; Bahrami, B.; Chowdhury, A. H.; Grimm, R. L.; Shi, Y.; Qiao, Q.; Zakeeruddin, S. M.; Gratzel, M.; Padture, N. P. High-performance

lead-free solar cells based on tin-halide perovskite thin films functionalized by a divalent organic cation. *ACS Energy Lett.* **2020**, *5*, 2223−2230.
(11) Jokar, E.; Cheng, P.-Y.; Lin, C.-Y.; Narra, S.; Shahbazi, S.; Diau, E. W.-G. Enhanced performance and stability of 3D/2D tin perovskite solar cells fabricated with a sequential solution deposition. *ACS Energy Lett.* **2021**, *6*, 485−492.
(12) Ran, C.; Gao, W.; Li, J.; Xi, J.; Li, L.; Dai, J.; Yang, Y.; Gao, X.; Dong, H.; Jiao, B.; Spanopoulos, I.; Malliakas, C. D.; Hou, X.; Kanatzidis, M. G.; Wu, Z. Conjugated organic cations enable efficient self-healing $FASnI_3$ solar cells. *Joule* **2019**, *3*, 3072−3087.
(13) Shao, S.; Liu, J.; Portale, G.; Fang, H. H.; Blake, G. R.; ten Brink, G. H.; Koster, L. J. A.; Loi, M. A. Highly reproducible Sn-based hybrid perovskite solar cells with 9% efficiency. *Adv. Energy Mater.* **2018**, *8*, 1702019.
(14) Wu, T.; Cui, D.; Liu, X.; Luo, X.; Su, H.; Segawa, H.; Zhang, Y.; Wang, Y.; Han, L. Additive engineering toward high-performance tin perovskite solar cells. *Solar RRL* **2021**, *5*, 2100034.
(15) Jokar, E.; Chien, C.-H.; Fathi, A.; Rameez, M.; Chang, Y.-H.; Diau, E. W.-G. Slow surface passivation and crystal relaxation with additives to improve device performance and durability for tin-based perovskite solar cells. *Energy Environ. Sci.* **2018**, *11*, 2353−2362.
(16) Li, B.; Chang, B.; Pan, L.; Li, Z.; Fu, L.; He, Z.; Yin, L. Tin-based defects and passivation strategies in tin-related perovskite solar cells. *ACS Energy Lett.* **2020**, *5*, 3752−3772.
(17) Wang, C.; Gu, F.; Zhao, Z.; Rao, H.; Qiu, Y.; Cai, Z.; Zhan, G.; Li, X.; Sun, B.; Yu, X.; Zhao, B.; Liu, Z.; Bian, Z.; Huang, C. Self-repairing tin-based perovskite solar cells with a breakthrough efficiency over 11%. *Adv. Mater.* **2020**, *32*, 1907623.
(18) Wu, T.; Liu, X.; He, X.; Wang, Y.; Meng, X.; Noda, T.; Yang, X.; Han, L. Efficient and stable tin-based perovskite solar cells by introducing π-conjugated Lewis base. *Sci. China: Chem.* **2020**, *63*, 107−115.
(19) Wu, T.; Cui, D.; Liu, X.; Meng, X.; Wang, Y.; Noda, T.; Segawa, H.; Yang, X.; Zhang, Y.; Han, L. Efficient and stable tin perovskite solar cells enabled by graded heterostructure of light-absorbing layer. *Solar RRL* **2020**, *4*, 2000240.
(20) He, X.; Wu, T.; Liu, X.; Wang, Y.; Meng, X.; Wu, J.; Noda, T.; Yang, X.; Moritomo, Y.; Segawa, H.; Han, L. Highly efficient tin perovskite solar cells achieved in a wide oxygen concentration range. *J. Mater. Chem. A* **2020**, *8*, 2760−2768.
(21) Nakamura, T.; Yakumaru, S.; Truong, M. A.; Kim, K.; Liu, J.; Hu, S.; Otsuka, K.; Hashimoto, R.; Murdey, R.; Sasamori, T.; Kim, H. D.; Ohkita, H.; Handa, T.; Kanemitsu, Y.; Wakamiya, A. Sn(IV)-free tin perovskite films realized by in situ Sn(0) nanoparticle treatment of the precursor solution. *Nat. Commun.* **2020**, *11*, 3008.
(22) Jiang, X.; Li, H.; Zhou, Q.; Wei, Q.; Wei, M.; Jiang, L.; Wang, Z.; Peng, Z.; Wang, F.; Zang, Z.; Xu, K.; Hou, Y.; Teale, S.; Zhou, W.; Si, R.; Gao, X.; Sargent, E. H.; Ning, Z. One-step synthesis of SnI_2·(DMSO) adducts for high-performance tin perovskite solar cells. *J. Am. Chem. Soc.* **2021**, *143*, 10970−10976.
(23) Liu, X.; Wu, T.; Chen, J.-Y.; Meng, X.; He, X.; Noda, T.; Chen, H.; Yang, X.; Segawa, H.; Wang, Y.; Han, L. Templated growth of $FASnI_3$ crystals for efficient tin perovskite solar cells. *Energy Environ. Sci.* **2020**, *13*, 2896−2902.
(24) Wang, C.; Zhang, Y.; Gu, F.; Zhao, Z.; Li, H.; Jiang, H.; Bian, Z.; Liu, Z. Illumination durability and high-efficiency Sn-based perovskite solar cell under coordinated control of phenylhydrazine and halogen ions. *Matter* **2021**, *4*, 709−721.
(25) Jiang, X.; Wang, F.; Wei, Q.; Li, H.; Shang, Y.; Zhou, W.; Wang, C.; Cheng, P.; Chen, Q.; Chen, L.; Ning, Z. Ultra-high open-circuit voltage of tin perovskite solar cells via an electron transporting layer design. *Nat. Commun.* **2020**, *11*, 1245.
(26) Jokar, E.; Chien, C. H.; Tsai, C. M.; Fathi, A.; Diau, E. W. G. Robust tin-based perovskite solar cells with hybrid organic cations to attain efficiency approaching 10%. *Adv. Mater.* **2019**, *31*, 1804835.
(27) Shahbazi, S.; Li, M.-Y.; Fathi, A.; Diau, E. W.-G. Realizing a cosolvent system for stable tin-based perovskite solar cells using a two-step deposition approach. *ACS Energy Lett.* **2020**, *5*, 2508−2511.
(28) Liu, X.; Wang, Y.; Wu, T.; He, X.; Meng, X.; Barbaud, J.; Chen, H.; Segawa, H.; Yang, X.; Han, L. Efficient and stable tin perovskite solar cells enabled by amorphous-polycrystalline structure. *Nat. Commun.* **2020**, *11*, 2678.
(29) Snaith, H. J.; Abate, A.; Ball, J. M.; Eperon, G. E.; Leijtens, T.; Noel, N. K.; Stranks, S. D.; Wang, J. T. W.; Wojciechowski, K.; Zhang, W. Anomalous hysteresis in perovskite solar cells. *J. Phys. Chem. Lett.* **2014**, *5*, 1511−1515.
(30) Richardson, G.; O'Kane, S. E. J.; Niemann, R. G.; Peltola, T. A.; Foster, J. M.; Cameron, P. J.; Walker, A. B. Can slow-moving ions explain hysteresis in the current−voltage curves of perovskite solar cells? *Energy Environ. Sci.* **2016**, *9*, 1476−1485.

https://doi.org/10.1021/acs.jpclett.1c03107
J. Phys. Chem. Lett. 2021, 12, 10106−10111